

Effect of the Size Distribution of Nanoscale Dispersed Particles on the Zener Drag Pressure

A.R. EIVANI, S. VALIPOUR, H. AHMED, J. ZHOU, and J. DUSZCZYK

In this article, a new relationship for the calculation of the Zener drag pressure is described in which the effect of the size distribution of nanoscale dispersed particles is taken into account, in addition to particle radius and volume fraction, which have been incorporated in the existing relationships. Microstructural observations indicated a clear correlation between the size distribution of dispersed particles and recrystallized grain sizes in the AA7020 aluminum alloy. However, the existing relationship to calculate the Zener drag pressure yielded a negligible difference of 0.016 pct between the two structures homogenized at different conditions resulting in totally different size distributions of nanoscale dispersed particles and, consequently, recrystallized grain sizes. The difference in the Zener drag pressure calculated by the application of the new relationship was 5.1 pct, being in line with the experimental observations of the recrystallized grain sizes. Mathematical investigations showed that the ratio of the Zener drag pressure from the new equation to that from the existing equation is maximized when the number densities of all the particles with different sizes are equal. This finding indicates that in the two structures with identical parameters except the size distribution of nanoscale dispersed particles, the one that possesses a broader size distribution of particles, *i.e.*, the number densities of particles with different sizes being equal, gives rise to a larger Zener drag pressure than that having a narrow size distribution of nanoscale dispersed particles, *i.e.*, most of the particles being in the same size range.

DOI: 10.1007/s11661-010-0452-7

© The Author(s) 2010. This article is published with open access at Springerlink.com

I. INTRODUCTION

DISPERSED second-phase particles exert a retarding force or pressure, named Zener drag, on the low- and high-angle grain boundaries, which significantly affects the recovery, recrystallization, and grain growth of deformed structures.^[1–10] It is commonly understood that the Zener drag pressure is a complex function of the interface, shape, size, interspacing, and volume fraction of dispersed particles.^[1,2]

One of the primary objectives of the homogenization treatment applied to direct-chill cast aluminum alloys before hot deformation is to create small dispersoids that act as recrystallization inhibitors during deformation and annealing or solution treatments.^[11] In 3XXX series aluminum alloys, *e.g.*, Mn-containing dispersoids formed during homogenization, play an important role in controlling the recrystallization behavior of the alloys.^[12,13] In 6XXX series aluminum alloys, the formation of different kinds of dispersoids, *i.e.*, Zr-,

Mn-, and Cr-containing ones, which play a role of recrystallization inhibition, has been investigated.^[14–18] In the case of 7XXX series aluminum alloys, the formation of Zr- and Sc-containing dispersoids has been a subject of interest for many years.^[19–21] For example, Robson *et al.*^[19,20] investigated the effect of Zr addition on the dispersoid formation and the fraction recrystallized after hot deformation. It was concluded that by using an optimum two-step homogenization treatment, a smaller fraction of recrystallization could be obtained. Robson^[21] also studied the effect of Sc on the formation of dispersoids, as Sc was expected to eliminate the dispersoid-free zones, as observed in scandium-free 7050, thus greatly increasing the recrystallization resistance. Other investigations showed that, in addition to the size, shape, and volume fraction of dispersed particles, their size distribution is dependent on the homogenization treatment. For example, Fuller and Seidman^[22,23] investigated the precipitation and the evolution of Al(Sc,Zr) particles in an Al-Sc-Zr alloy during heat treatment and found these particles with different size distributions after different treatments. The results obtained by Clouet *et al.*^[24] also clearly showed that quite different size distributions of Al₃Zr and Al₃Sc particles ranging from a broad distribution to a localized one might result from different treatments employed. Similar observations were made by Li and Arnberg^[25] as to the formation of Mn-rich dispersoids in the AA3003 aluminum alloy and by Novotny and Ardell^[26] concerning the formation of Al₃Sc particles in an Al-Sc alloy.

A.R. EIVANI, Researcher, is with the Materials Innovation Institute, 2628 CD Delft, The Netherlands, and the School of Metallurgical and Materials Engineering, Iran University of Science and Technology (IUST), Tehran, Iran. Contact e-mail: a.eivani@m2i.nl S. VALIPOUR, Researcher, is with the School of Science, Razi University, Kermanshah, Iran. H. AHMED, Researcher, is with the Materials Innovation Institute. J. ZHOU and J. DUSZCZYK, Associate Professors, are with the Department of Materials Science and Engineering, Delft University of Technology, 2628 CD Delft, The Netherlands.

Manuscript submitted May 7, 2009.

Article published online November 17, 2010

Considering a random spatial correlation between the boundaries and the dispersed particles, the Zener drag pressure (P_z) can be expressed in the simplest form by the following relationship:^[1,2]

$$P_z = \frac{3\gamma F_v}{2r} \quad [1]$$

where F_v is the local volume fraction of dispersed particles, r the particle radius, and γ the energy of the grain boundary that dispersed particles are pinning. It can be seen from Eq. [1] that the Zener drag due to the presence of dispersed particles at grain boundaries is maximized by maximizing the volume fraction (F_v) and minimizing the particle size (r).

There are also some interesting publications on the effect of Zener drag pressure on the recrystallization behavior. For example, Nes *et al.*^[2] studied the interactions between particles and grain boundaries, including the effects of the size, shape, and distribution of the particles with the same size, and found that such effects may strongly affect the recrystallization and grain growth. However, the authors did not consider the effect of the size distribution of particles. Andersen and Grong^[27,28] proposed an analytical model of grain growth in metals and alloys in the presence of growing and dissolving precipitates on normal^[27] and abnormal^[28] grain growth. Novikov^[29] simulated the grain growth in three-dimensional model polycrystals with randomly distributed particles at the grain boundaries. The particles were assumed to be of spherical shape and identical sizes, and their boundaries to be noncoherent. Simulations yielded the exact dependence of the normalized limiting grain size on the particle volume fraction, regardless of the initial grain size.^[29] It was concluded that in materials with randomly distributed particles, the dependence of the normalized limiting grain size on the volume fraction is tight up to a volume fraction of 0.12, which proved the validity of the Zener theory as well as their simulations. Maazi and Rouag^[30] presented a model for grain growth simulation, in the presence of a preferential particle distribution. The model predicted two grain size limits due to second-phase particles. If the particles had a size less than the maximal critical radius, the grains would shrink, and if these had a size greater than the minimal critical radius, the grains would grow, while between the two limiting radii, no grain growth took place. In most of the studies in this field, the basic equation of Eq. [1] and its derivations^[6-9] have been used to estimate the retarding pressure for recrystallization, and a reasonable agreement between the predictions and the experimental results has been reached. Further studies^[8,11,12] on the Zener drag without introducing other effective parameters such as the size distribution of dispersed particles have not led to any relationship that is significantly different from Eq. [1].

In other studies, however, the size distribution of dispersed particles has been recognized as an effective parameter on the physical and mechanical behavior of materials. For example, the effect of the size distribution of dispersed particles on the mechanical properties and the growth and dissolution of these particles in structures were investigated.^[31-36] Myhr *et al.*^[33] generated a

special control volume formulation of the classical precipitation model for coupled nucleation, growth, and coarsening to describe the evolution of the particle size distribution with time during thermal processing of Al-Mg-Si alloys, including both isothermal and nonisothermal transformation behavior. The size distribution of particles was found to be effective on the precipitation behavior. Myhr and Grong^[34] studied the nonisothermal transformations in alloys containing a distribution of particles and found that the memory of a past process step, *i.e.*, the previous particle sizes, is likely to have an effect on the overall transformation behavior. In addition, Tundal and Ryum^[35,36] investigated the effect of size distribution of dispersed particles on their dissolution during homogenization. It was demonstrated that the size distribution of particles is an effective parameter on the model predictions and, therefore, should be considered in the model if an accurate prediction of the dissolution kinetics is to be achieved. However, there has been no publication on the effect of size distribution of dispersed particles on the recrystallization behavior. In other words, no study has been conducted with the effect of this parameter on the Zener drag pressure taken into account, although it is experimentally observed that this effect is partly responsible for recrystallization and grain growth behavior.

In this article, two heating rates toward a homogenization temperature were chosen in order to create two distinctively different size distributions of dispersed particles with similar values of P_z based on Eq. [1]. The samples were then hot deformed, followed by annealing to demonstrate a relationship between the size distribution of dispersed particles and the recrystallized grain size in the AA7020 aluminum alloy. The objective of this research was to derive a new relationship that included the effect of the size distribution of dispersed particles in the calculation of the Zener drag pressure. The derived equation could then be used to suggest an optimum size distribution of dispersed particles, which would result in a maximum Zener drag pressure.

II. EXPERIMENTAL PROCEDURE

Cubic samples of 20 mm were cut from the center of a direct chill cast AA7020 ingot. The chemical composition of the samples used in this study is shown in Table I. The as-cast samples were homogenized at 783 K (510 °C) for 8 hours prior to which two different heating rates of 523 K and 323 K/h (250 °C and 50 °C/h) were applied and coded as S1 and S2. After the homogenization treatment, the samples were cooled in air.

The as-homogenized samples were examined using a JEOL* 6500 field emission gun-scanning electron

*JEOL is a trademark of Japan Electron Optics Ltd., Tokyo.

microscope (FEG-SEM). The optimum operating voltage and current were found to be 10 kV and 1 nA, respectively. To estimate the number density of

nanoscale dispersed particles, images at a magnification of 50,000 were examined using image analysis, while for the determination of the sizes of the dispersed particles, a magnification of 75,000 was used in order to ensure accuracy.

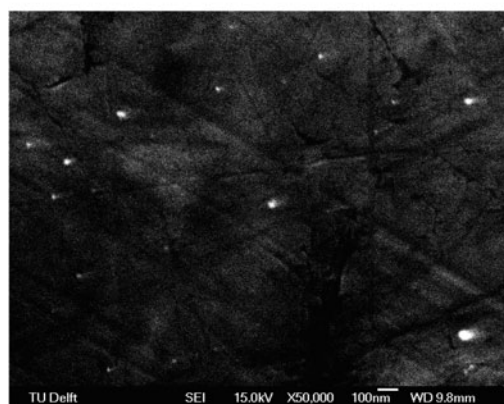
Uniaxial hot compression tests were performed at 723 K (450 °C) at a strain rate of 10 s^{-1} , using a DSI GLEEBLE** 3800 thermomechanical simulator.

**GLEEBLE is a trademark of DSI, Inc., Poestenskill, NY.

Compressive deformation proceeded to a strain of 0.6. The tests were performed at least twice for each condition to ensure the repeatability of the data. Cylindrical samples having a diameter of 10 mm and a length of 12 mm were used. They were heated to 723 K (450 °C) at a heating rate of 10 K/s (10 °C/s) and kept at the temperature for 110 seconds in order to attain a homogenous temperature in the test material and anvils, based on the previous studies using the same facility.^[37] The samples were subsequently water quenched to maintain the as-deformed structure so that no further microstructural changes would occur after deformation. The samples were annealed in a salt bath furnace at 773 K (500 °C) for 2 hours and then cut through thickness. The grain structure was studied by a polarized light optical microscope. The average grain size from five images was determined using the general line intercept procedure according to ASTM E 112-96.^[38]

Table I. Chemical Composition of the Alloy Used in this Study

Element	Si	Fe	Cu	Mn	Mg	Zn	Ti	Cr	Zr	Al
Wt pct	0.30	0.30	0.19	0.35	1.20	4.37	0.002	0.10	0.13	bal.



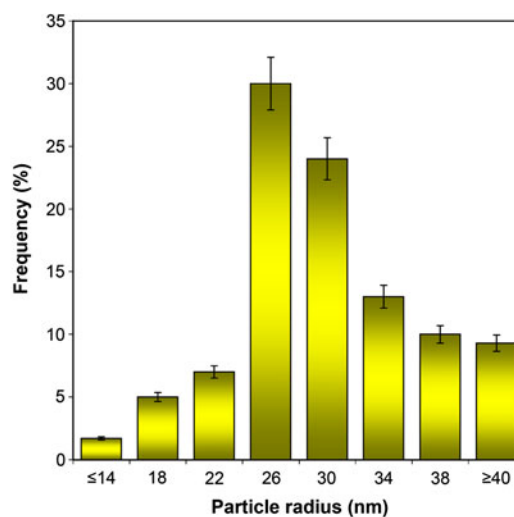
(a)

III. RESULTS AND DISCUSSION

A. Effective Parameters on the Recrystallization Resistance and Grain Growth

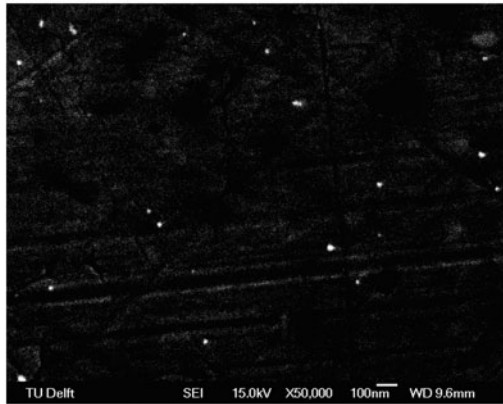
The ability of FEG-SEM to determine the sizes of dispersoids of larger than 10 nm in AA7050 has been reported.^[19] In addition, it has been confirmed by the present authors in the case of AA7020^[39] that the particle radii measured using both FEG-SEM and transmission electron microscopy imaging methods are in quite reasonable agreement. However, the FEG-SEM is easier to use and gives the possibility of investigating a larger area of sample for statistical measurements and was thus used exclusively in this investigation.

Figures 1(a) and 2(a) present typical FEG-SEM images of samples S1 and S2, respectively. The white spots clearly seen in the images are the dispersed particles, which have distinctly different distributions as a result of the different homogenization conditions. The size distributions of the particles are shown in Figures 1(b) and 2(b). It can be seen that these two structures indeed contain dispersed particles of quite different size distributions. It should be mentioned that the sizes of individual particles in each image were measured by taking pictures at higher magnifications under the SEM. In sample S1, most of the particles fall in a narrow size range of 26 to 30 nm, while in sample S2, the number densities of the particles with different sizes from 14 to 40 nm are almost equal. The main reason for these two different particle size distributions is the different heating rates applied during homogenization from room temperature to the homogenization temperature. At the faster heating rate, sample S1, the material was taken to the homogenization temperature within a short period of time, about 1 hour. In this case, most of the dispersoids formed at higher temperatures, near or at 783 K (510 °C). At these temperatures, the critical radius for a new nucleus to form is larger than at

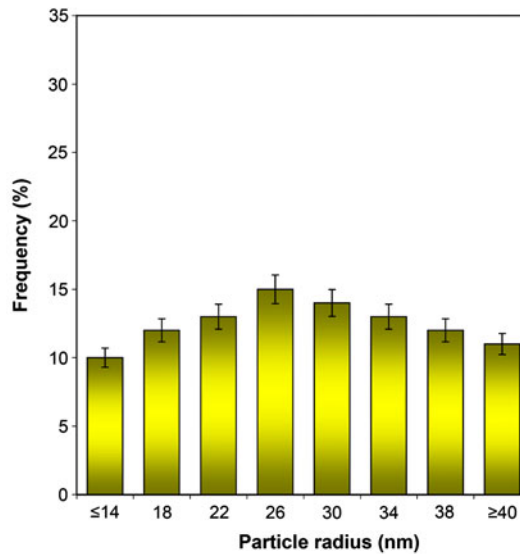


(b)

Fig. 1—(a) FEG-SEM image of the sample S1 after the homogenization treatment and (b) average size distribution of the nanoscale dispersed particles determined from 25 images. $N = 5.3 \mu\text{m}^{-2}$ ($N = 12.2 \mu\text{m}^{-3}$) and $r_{\text{avg}} = 30 \text{ nm}$.



(a)



(b)

Fig. 2—(a) FEG-SEM image of the sample S2 after the homogenization treatment and (b) average size distribution of the nanoscale dispersed particles determined from 25 images. $N = 5.94 \mu\text{m}^{-2}$ ($N = 14.48 \mu\text{m}^{-3}$) and $r_{\text{avg}} = 28 \text{ nm}$.

Table II. Number Densities and Average Radii of Nanoscale Dispersed Particles, along with the Calculated P_z/γ Values Using Equation [1]

Sample Name	$N (\mu\text{m}^{-3})$	$r_{\text{avg}} (\text{nm})$	$P_z/\gamma (\mu\text{m}^{-1})$	Difference in P_z/γ (Pct)
S1	12.20	30	0.06894	0.016
S2	14.48	28	0.06895	

lower temperatures.^[40–42] It is possible that some of the nuclei that formed during heating would dissolve in the structure, since at the homogenization temperature, they might not be stable at 783 K (510 °C). Such behavior has been observed in the case of the formation of precipitates during age hardening of aluminum alloys.^[33–36] Therefore, only the particles that had sufficiently large sizes could survive and continue to grow, which resulted in a narrow size distribution of particles. In addition, due to the very short time to reach the homogenization temperature, the fraction of the particles that formed during heating might not be significant. Therefore, most of the particles formed near or at the homogenization temperature and, consequently, had almost the same sizes. However, at the lower heating rate, sample S2 was at low temperatures for a longer time during heating, about 10 hours compared to 1 hour for S1. Particles having different sizes would form during heating and became stable before reaching the homogenization temperature. Consequently, sample S2 had almost equal number densities of particles with different sizes.

The average particle radii and number densities are shown in Table II, which also presents the average normalized values of the Zener drag pressure (P_z/γ), calculated using Eq. [1]. It is clear that although these two microstructures contain dispersed particles with quite different size distributions, Eq. [1] results in very

similar P_z/γ values with a difference as small as 0.016 pct. (This value has been calculated as the percentage difference between the values of P_z/γ in samples S1 and S2.)

To verify the viability of the existing relationship, Eq. [1], to calculate the Zener drag pressure, the recrystallization response of the samples after hot deformation and annealing was investigated and the results are shown in Figures 3(a) and (b) for the samples S1 and S2, respectively. It is clear that the sample S2 heated at a slower rate to the homogenization temperature of 783 K (510 °C) has smaller recrystallized grains. S2 has an average grain size of $54 \pm 5 \mu\text{m}$, while S1 has an average grain size of $73 \pm 7 \mu\text{m}$.

It is well known that the interface, shape, size, interspacing, and volume fraction of dispersed particles^[1,2] affect the Zener drag pressure and, therefore, the recrystallization resistance and grain growth of a deformed material. The Zener drag pressure exerted by dispersed particles shown in Eq. [1] represents the easiest way to judge the recrystallization resistance of the deformed material. However, the results of the present investigation clearly show that in spite of the similar values of the Zener drag pressure based on the existing relationship (Eq. [1]), the recrystallization response is quite different. This indicates that in addition to the mentioned parameters, the size distribution of dispersed particles may also be effective on the recrystallization resistance.

B. The Zener Drag Relationship Including the Effect of the Size Distribution of Dispersed Particles

The procedure to calculate the Zener drag pressure including the size distribution of particles was the same as that used in References^[1] and^[2]. Assuming that the boundary is planar,^[1,2] the particle within a distance r_i

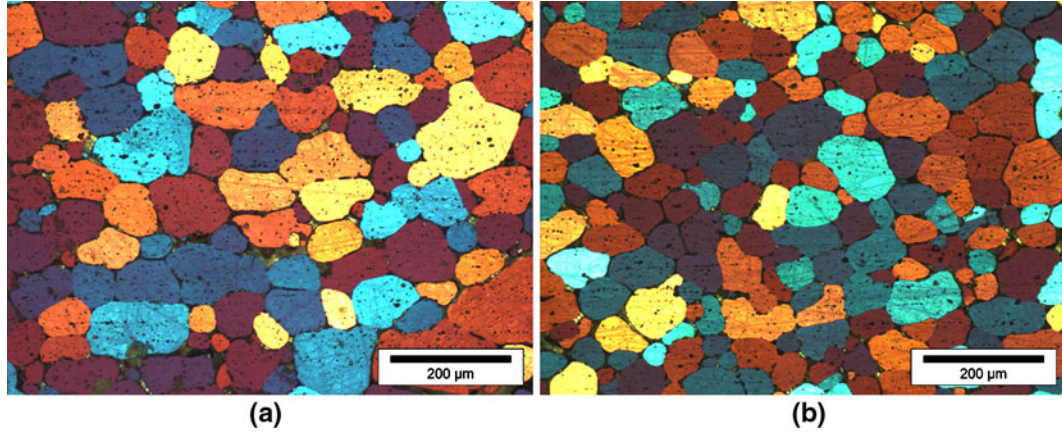


Fig. 3—Grain structure after annealing at 848 K (575 °C) for 10 min, following hot compression tests of the samples (a) S1 and (b) S2.

on either side of the boundary will intersect it. Therefore, N_{Si} , the number of particles intersecting with a unit area of the boundary for the particles with a size of r_i , is^[1,2]

$$N_{Si} = 2r_i N_{Vi} \quad [2]$$

where N_{Vi} is the number of particles with a radius of r_i per unit volume. The pinning pressure exerted on the unit area of the boundary by the particles with a size of r_i (P_{Zi}) is given by^[1,2]

$$P_{Zi} = N_{Si} F_{Si} \quad [3]$$

in which, the maximum restraining force on the boundary, F_{Si} , can be expressed as^[1,2]

$$F_{Si} = \pi r_i \gamma \quad [4]$$

where γ is the specific energy of the boundaries that the particles pin. Equation [3] may be rewritten as^[1,2]

$$P_{Zi} = N_{Si} \pi r_i \gamma \quad [5]$$

Inserting Eq. [2] into Eq. [5] leads to

$$P_{Zi} = 2N_{Vi} \pi r_i^2 \gamma \quad [6]$$

Therefore, the pressure exerted on a boundary by a group of particles with different sizes is

$$P_Z = 2\pi\gamma \sum_{i=1}^n N_{Vi} r_i^2 \quad [7]$$

By inserting the relationship between the number density of particles, their radii, and the volume fraction presented in Eq. [8]^[1,2] into Eq. [7], Eq. [9] is derived.

$$N_{Vi} = \frac{3F_{Vi}}{4\pi r_i^3} \quad [8]$$

$$P_Z = \frac{3}{2}\gamma \sum_{i=1}^n \frac{F_{Vi}}{r_i} \quad [9]$$

Table III shows the calculated normalized values of the Zener drag pressure (P_z/γ) for samples S1 and S2,

Table III. Calculated P_z/γ Values for Samples S1 and S2 Using Equation [9]

Sample Name	P_z/γ (μm^{-1})	Difference in P_z/γ (Pct)
S1	0.0726	5.1
S2	0.0763	—

based on Eq. [7]. It is clear that the newly derived equation predicts a larger value of P_z/γ for sample S2, being 5.1 pct larger than that of sample S1, which is in line with the experimental observations in this research. As mentioned earlier, the percentage is expressed by the percentage difference between the values of P_z/γ in samples S1 and S2.

C. Differences between the Existing and the Newly Derived Equations

Based on Eq. [9], it is clear that the newly derived equation is inherently close to the existing one, Eq. [1]. However, Eq. [9] gives the possibility to differentiate between different size distributions of particles to obtain the highest recrystallization inhibition. The term α is defined as the ratio of the Zener drag pressure including the effect of the size distribution of dispersed particles to the Zener drag pressure without this effect. For the α parameter, the Zener drag pressure was calculated using the average radius of the dispersed particles, following the same procedure, which resulted in

$$P_{Z\text{avg}} = 2\pi\gamma N_{V\text{avg}} r_{\text{avg}}^2 \quad [10]$$

where

$$N_{V\text{avg}} = \sum_{i=1}^n N_{Vi} \quad [11]$$

and

$$r_{\text{avg}} = \frac{\sum_{i=1}^n N_{Vi} r_i}{\sum_{i=1}^n N_{Vi}} \quad [12]$$

Therefore, substituting the terms in Eq. [10] with Eqs. [11] and [12] yields a P_z value equal to

$$P_{Zavg} = 2\pi\gamma \frac{\left(\sum_{i=1}^n N_{Vi}r_i\right)^2}{\sum_{i=1}^n N_{Vi}} \quad [13]$$

The α parameter is

$$\alpha = \frac{P_Z}{P_{Zavg}} = \frac{\sum_{i=1}^n N_{Vi}r_i^2 \sum_{i=1}^n N_{Vi}}{\left(\sum_{i=1}^n N_{Vi}r_i\right)^2} \quad [14]$$

With mathematical simplification, Eq. [14] may be rewritten as

$$\alpha = \frac{\left(\sum_{i=1}^n N_{Vi}r_i\right)^2 + \sum_{i=1}^{n-1} \left(N_{Vi} \sum_{j=i+1}^n N_{Vj}(r_i - r_j)^2\right)}{\left(\sum_{i=1}^n N_{Vi}r_i\right)^2} \quad [15]$$

The detailed expressions of the individual terms in Eq. [15] are presented in Appendix A. Assuming the dispersed particles with different sizes are at a constant size difference equal to d , *i.e.*, $(r_{i+1} - r_i) = d$, α may be expressed as

$$\alpha = \frac{\left(\sum_{i=1}^n N_{Vi}r_i\right)^2 + d^2 \sum_{i=1}^{n-1} \left(N_{Vi} \sum_{j=i+1}^n N_{Vj}\right)}{\left(\sum_{i=1}^n N_{Vi}r_i\right)^2} \quad [16]$$

It is clear that the first term of the numerator in Eq. [16] is equal to the denominator. Therefore, the determining term for the maximization of the α parameter is the second term of the numerator defined as NUM.

$$NUM = d^2 \sum_{i=1}^{n-1} \left(N_{Vi} \sum_{j=i+1}^n N_{Vj}\right) \quad [17]$$

Since all the terms in Eq. [16] are positive, α is always larger than 1. This finding indicates that the newly derived equation for the Zener drag pressure always has a larger value than the one using the average particle size values. This may be considered an advantage over the P_z calculated from the average values, since it is always less than the values predicted by the equation according to the size distribution of particles. In other words, it is a trustable equation to rely on for inhibiting recrystallization. As presented in Appendix B, NUM will be maximized when the number densities of the particles of different sizes are equal, which may be written as

$$N_1 = N_2 = \dots = N_{max} = \dots = N_{n-1} = N_n \quad [18]$$

Equation [18] indicates that for a given total number density of evenly dispersed particles, P_z is maximized when the particles with different sizes have equal

number densities, as indicated by a broad distribution of particle sizes in the size distribution plot. This is in agreement with the finding in this research that the recrystallization resistance of sample S2 with a broader size distribution of particles, as shown in Figure 2(b), is larger. The corresponding values of the α parameter for samples S1 and S2 were calculated to be 1.05 and 1.11, respectively.

IV. CONCLUSIONS

In this study, two different homogenization treatments were applied, resulting in distinctively different size distributions of dispersed particles. However, the Zener drag pressure values based on the existing equation showed only a very small difference of 0.016 pct, although the recrystallized grain sizes after hot deformation and subsequent annealing were quite different. A new relationship for the Zener drag pressure was derived, which accounted for the effect of the size distribution of dispersed particles. The predictions of the newly derived equation were compared to the recrystallized grain sizes after hot compression and subsequent annealing. The following conclusions have been drawn.

1. In addition to the known parameters, *i.e.*, the interface, shape, size, interspacing, and volume fraction of dispersed particles, the size distribution of particles is also an effective parameter on the recrystallization inhibition of the alloy.
2. The newly developed equation is able to differentiate between the samples with similar P_z values from the average particle radii, but with different size distributions of dispersed particles.
3. The ratio of the Zener drag pressure from the new equation to that from the existing equation is maximized when the number densities of all the particles with different sizes are equal. This indicates that in the two structures with identical parameters except the size distribution of dispersed particles, the one that possesses a broader size distribution of particles, *i.e.*, the number densities of particles with different sizes being equal, gives rise to a larger Zener drag pressure than that having a narrow size distribution of dispersed particles, *i.e.*, most of the particles being in the same small size range.

ACKNOWLEDGMENT

This research was carried out under Project No. MC 4.04203 in the framework of the Research Program of the Materials innovation institute M2i (www.m2i.nl).

OPEN ACCESS

This article is distributed under the terms of the Creative Commons Attribution Noncommercial License which permits any noncommercial use, distribution, and reproduction in any medium, provided the original author(s) and source are credited.

APPENDIX A

For the α parameter, Eq. [14] may be written as

$$\alpha = \frac{\{(N_1 r_1^2 + N_2 r_2^2 + N_3 r_3^2 + \dots + N_n r_n^2) (N_1 + N_2 + N_3 + \dots + N_n)\}}{\left(\sum_{i=1}^n N_{Vi} r_i\right)^2} \quad [\text{A1}]$$

Multiplication in the numerator of Eq. [A1] leads to

$$\alpha = \frac{\{(N_1^2 r_1^2 + N_2^2 r_2^2 + N_3^2 r_3^2 + \dots + N_n^2 r_n^2) + (N_1 N_2 r_1^2 + N_1 N_3 r_1^2 + \dots + N_1 N_n r_1^2) + \dots + (N_n N_1 r_n^2 + N_n N_2 r_n^2 + \dots + N_n N_{n-1} r_n^2)\}}{\left(\sum_{i=1}^n N_{Vi} r_i\right)^2} \quad [\text{A2}]$$

Equation [A2] can be ordered as

$$\alpha = \left\{ \begin{aligned} &\left(\begin{array}{l} N_1^2 r_1^2 \\ + N_2^2 r_2^2 \\ + N_3^2 r_3^2 \\ + \dots \\ + N_n^2 r_n^2 \end{array} \right) + \left(\begin{array}{l} N_1 N_2 (r_1^2 + r_2^2) \\ + N_1 N_3 (r_1^2 + r_3^2) \\ + \dots \\ + N_1 N_n (r_1^2 + r_n^2) \end{array} \right) \\ &+ \left(\begin{array}{l} N_2 N_3 (r_2^2 + r_3^2) \\ + N_2 N_4 (r_2^2 + r_4^2) \\ + \dots \\ + N_2 N_n (r_2^2 + r_n^2) \end{array} \right) + \left(\begin{array}{l} N_3 N_4 (r_3^2 + r_4^2) \\ + N_3 N_5 (r_3^2 + r_5^2) \\ + \dots \\ + N_3 N_n (r_3^2 + r_n^2) \end{array} \right) \\ &+ \dots + N_{n-1} N_n (r_{n-1}^2 + r_n^2) \end{aligned} \right\} / \left(\sum_{i=1}^n N_{Vi} r_i\right)^2 \quad [\text{A3}]$$

which can be rearranged as

$$\alpha = \frac{\{(N_1^2 r_1^2 + N_2^2 r_2^2 + N_3^2 r_3^2 + \dots + N_n^2 r_n^2) + (2N_1 N_2 r_1 r_2 + 2N_1 N_3 r_1 r_3 + \dots + 2N_1 N_n r_1 r_n) + (2N_2 N_3 r_2 r_3 + 2N_2 N_4 r_2 r_4 + \dots + 2N_2 N_n r_2 r_n) + (2N_3 N_4 r_3 r_4 + 2N_3 N_5 r_3 r_5 + \dots + 2N_3 N_n r_3 r_n) + \dots + 2N_{n-1} N_n r_{n-1} r_n\} + \{(N_1 N_2 (r_1 - r_2)^2 + N_1 N_3 (r_1 - r_3)^2 + \dots + N_1 N_n (r_1 - r_n)^2) + (N_2 N_3 (r_2 - r_3)^2 + N_2 N_4 (r_2 - r_4)^2 + \dots + N_2 N_n (r_2 - r_n)^2) + (N_3 N_4 (r_3 - r_4)^2 + N_3 N_5 (r_3 - r_5)^2 + \dots + N_3 N_n (r_3 - r_n)^2) + \dots + N_{n-1} N_n (r_{n-1} - r_n)^2\}}{\left(\sum_{i=1}^n N_{Vi} r_i\right)^2} \quad [\text{A4}]$$

or

$$\alpha = \frac{\left\{ \left(\sum_{i=1}^n N_{Vi} r_i\right)^2 + (N_1 N_2 (r_1 - r_2)^2 + N_1 N_3 (r_1 - r_3)^2 + \dots + N_1 N_n (r_1 - r_n)^2) + (N_2 N_3 (r_2 - r_3)^2 + N_2 N_4 (r_2 - r_4)^2 + \dots + N_2 N_n (r_2 - r_n)^2) + (N_3 N_4 (r_3 - r_4)^2 + N_3 N_5 (r_3 - r_5)^2 + \dots + N_3 N_n (r_3 - r_n)^2) + \dots + N_{n-1} N_n (r_{n-1} - r_n)^2 \right\}}{\left(\sum_{i=1}^n N_{Vi} r_i\right)^2} \quad [\text{A5}]$$

Eq. [A5] can be mathematically simplified as

$$\alpha = \frac{\left(\sum_{i=1}^n N_{Vi} r_i\right)^2 + \sum_{i=1}^{n-1} \left(N_{Vi} \sum_{j=i+1}^n N_{Vj} (r_i - r_j)^2\right)}{\left(\sum_{i=1}^n N_{Vi} r_i\right)^2} \quad [\text{A6}]$$

Assuming the dispersed particles with different sizes are evenly sized with a difference equal to d , i.e., $(r_i - r_{i+1}) = d = cte$.

$$\alpha = \frac{\left(\sum_{i=1}^n N_{Vi} r_i\right)^2 + d^2 \sum_{i=1}^{n-1} \left(N_{Vi} \sum_{j=i+1}^n N_{Vj}\right)}{\left(\sum_{i=1}^n N_{Vi} r_i\right)^2} \quad [\text{A7}]$$

APPENDIX B

Assuming the total number density of dispersed particles is N_{tot} , which can be written as

$$N_{tot} = N_1 + N_2 + \dots + N_{max} + \dots + N_{n-1} + N_n \quad [\text{B1}]$$

where N_{max} is the largest number density of dispersed particles with a specific size, Eq. [B2] expressing the ratio of other number densities to the maximum number densities can be written as

$$N_{max} = \frac{1}{m_1} N_1 = \frac{1}{m_2} N_2 = \dots = \frac{1}{m_{n-1}} N_{n-1} = \frac{1}{m_n} N_n \quad [\text{B2}]$$

The numbers m_1, m_2, \dots, m_{n-1} and m_n should be less than 1, since N_{max} is larger than all the other values of N , i.e., N_1 to N_n . Since the number density cannot have a negative value, m_1, m_2, \dots, m_{n-1} , and m_n should be larger than zero. Equation [B2] can be extended as

$$\begin{aligned} \text{NUM} = & d^2[(N_1N_2 + N_1N_3 + \dots + N_1N_n) \\ & + (N_2N_3 + N_2N_4 + \dots + N_2N_n) \\ & + (N_3N_4 + N_3N_5 + \dots + N_3N_n) \\ & + \dots + N_{n-1}N_n] \end{aligned} \quad [\text{B3}]$$

Insertion of N_{\max} into Eq. [B3] yields

$$\begin{aligned} \text{NUM} = & d^2 N_{\max}^2 ((m_1m_2 + m_1m_3 + \dots + m_1m_n) \\ & + (m_2m_3 + m_2m_4 + \dots + m_2m_n) \\ & + (m_3m_4 + m_3m_5 + \dots + m_3m_n) \\ & + \dots + m_{n-1}m_n) \end{aligned} \quad [\text{B4}]$$

NUM in Eq. [B3] will be maximized if $m_1 = m_2 = \dots = m_n = 1$, since m_1 to m_n are between 0 and 1. By giving 1 for all m_1 to m_n in Eq. [B2], it becomes

$$N_{\max} = N_1 = N_2 = \dots = N_{n-1} = N_n \quad [\text{B5}]$$

This indicates that for a given total number density of evenly sized dispersed particles with a constant difference in size, P_z will be maximized when the particles with different sizes have equal number densities.

REFERENCES

1. F.J. Humphreys and M. Hatherly: *Recrystallization and Related Annealing Phenomena*, Elsevier Science, Inc., Oxford, United Kingdom, 1995, pp. 109–14.
2. E. Nes, N. Ryum, and O. Hunderi: *Acta Metall.*, 1985, vol. 33, pp. 11–22.
3. M. Jones and F.J. Humphreys: *Acta Mater.*, 2003, vol. 51, pp. 2149–59.
4. M. Ferry: *Acta Mater.*, 2005, vol. 53, pp. 773–873.
5. C.S. Smith: *Trans. TMS-AIME*, 1948, vol. 175, pp. 15–51.
6. M.F. Ashby, J. Harper, and J. Lewis: *Trans. TMS-AIME*, 1969, vol. 245, pp. 413–20.
7. R.D. Doherty, D.A. Hughes, F.J. Humphreys, J.J. Jonas, D. Juul Jensen, D.E. Kassner, W.E. King, T.R. McNelley, H.J. McQueen, and A.D. Rollett: *Mater. Sci. Eng.*, 1997, vol. 238, pp. 219–74.
8. M. Hillert: *Acta Metall.*, 1965, vol. 13, pp. 227–38.
9. F.J. Humphreys and M.G. Ardakani: *Acta Mater.*, 1996, vol. 44, pp. 2717–27.
10. F.J. Humphreys: *Acta Mater.*, 1997, vol. 45, pp. 5031–39.
11. T. Sheppard: *Extrusion of Aluminum Alloys*, Kluwer Academic Publishers, Dordrecht, The Netherlands, 1999, pp. 227–52.
12. M. Peters, J. Eschweiler, and K. Welpmann: *Scripta Metall.*, 1986, vol. 20, pp. 259–64.
13. O. Daaland and E. Nes: *Acta Mater.*, 1996, vol. 44, pp. 1389–1411.
14. L. Lodgaard and N. Ryum: *Mater. Sci. Eng. A*, 2000, vol. 283, pp. 144–52.
15. M. Cabibbo, E. Evangelista, C. Scalabroni, and E. Bonetti: *Mater. Sci. Forum*, 2006, vols. 503–504, pp. 841–46.
16. L. Lodgaard and N. Ryum: *Mater. Sci. Technol.*, 2000, vol. 16, pp. 599–604.
17. D.H. Lee, J.H. Park, and S.W. Nam: *Mater. Sci. Technol.*, 1999, vol. 15, pp. 450–55.
18. R.A. Jeniski, B. Thanaboonsombut, and T.H. Sanders: *Metall. Mater. Trans. A*, 1996, vol. 27A, pp. 19–27.
19. J.D. Robson and P.B. Prangnell: *Acta Mater.*, 2001, vol. 49, pp. 599–613.
20. J.D. Robson: *Mater. Sci. Eng. A*, 2002, vol. 338, pp. 219–29.
21. J.D. Robson: *Acta Mater.*, 2004, vol. 52, pp. 1409–21.
22. C.B. Fuller and D.N. Seidman: *Acta Mater.*, 2005, vol. 53, pp. 5401–13.
23. C.B. Fuller and D.N. Seidman: *Acta Mater.*, 2005, vol. 53, pp. 5415–28.
24. E. Clouet, A. Barbu, L. Lae, and G. Martin: *Acta Mater.*, 2005, vol. 53, pp. 2313–25.
25. Y.J. Li and L. Arnberg: *Acta Mater.*, 2003, vol. 51, pp. 3415–28.
26. G.M. Novotny and A.J. Ardell: *Mater. Sci. Eng. A*, 2001, vol. 318, pp. 144–54.
27. I. Andersen and Ø. Grong: *Acta Metall. Mater.*, 1995, vol. 43, pp. 2673–88.
28. I. Andersen and Ø. Grong: *Acta Metall. Mater.*, 1995, vol. 43, pp. 2689–2700.
29. V.Y. Novikov: *Scripta Mater.*, 2000, vol. 42, pp. 439–43.
30. N. Maazi and N.J. Rouag: *Cryst. Growth*, 2002, vol. 243, pp. 361–69.
31. E. Nes: *Proc. Symp. on Microstructural Control during Processing of Aluminum Alloys*, New York, NY, 1985, pp. 95–102.
32. R.D. Doherty, D.J. Srolovitz, A.R. Rollet, and M.P. Anderson: *Scr. Metall.*, 1987, vol. 21, pp. 675–79.
33. O.R. Myhr, Ø. Grong, and S.J. Andersen: *Acta Mater.*, 2001, vol. 49, pp. 65–75.
34. O.R. Myhr and Ø. Grong: *Acta Mater.*, 2000, vol. 48, pp. 1605–15.
35. U.H. Tundal and N. Ryum: *Metall. Trans. A*, 1992, vol. 23A, pp. 433–49.
36. U.H. Tundal and N. Ryum: *Metall. Trans. A*, 1992, vol. 23A, pp. 445–49.
37. F.A. Sloof, J. Zhou, and J. Duszczyk: *7th Int. Conf. Magnesium Alloys and Their Applications*, Wiley-VCH, Weinheim, Germany, 2006, pp. 324–29.
38. “ASTM E 112-96 Standard Test Methods for Determining Average Grain Size,” *Annual Book of ASTM Standards*, ASTM International, West Conshohocken, PA, 2004, vol. 03.01, pp. 1–26.
39. A.R. Eivani, H. Ahmed, J. Zhou, J. Duszczyk, and C. Kwakernaak: *Mater. Sci. Technol.*, 2010, in press, DOI 10.1179/026708310X12635619988267.
40. J.W. Martin: *Precipitation Hardening*, 2nd ed., Butterworth-Heinemann, Oxford, United Kingdom, 1998, pp. 79–111.
41. D.A. Porter and K.E. Easterling: *Phase Transformation in Metals and Alloys*, VNR International, London, 1981, pp. 263–381.
42. R.W. Cahn and P. Haasen: *Physical Metallurgy*, 4th ed., Elsevier Science BV, North Holland, the Netherlands, 1996, pp. 1363–1400.